

The Tuberculosis Prodrug Isoniazid Bound to Activating Peroxidases*

Received for publication, September 4, 2007, and in revised form, October 29, 2007 Published, JBC Papers in Press, December 5, 2007, DOI 10.1074/jbc.M707412200

Clive Metcalfe[‡], Isabel K. Macdonald^{‡1}, Emma J. Murphy[‡], Katherine A. Brown[§], Emma Lloyd Raven[‡], and Peter C. E. Moody^{¶1,2}

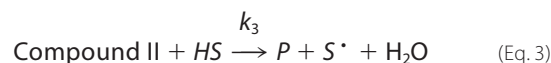
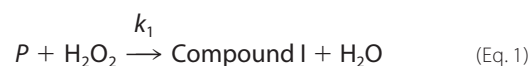
From the Departments of [‡]Chemistry and [¶]Biochemistry, University of Leicester, Lancaster Road, Leicester LE1 9HN and [§]Department of Life Sciences, Division of Cell and Molecular Biology, Centre for Molecular Microbiology and Infection, Imperial College, Exhibition Road, London SW7 2AZ, United Kingdom

Isoniazid (INH, isonicotinic acid hydrazine) is one of only two therapeutic agents effective in treating tuberculosis. This prodrug is activated by the heme enzyme catalase peroxidase (KatG) endogenous to *Mycobacterium tuberculosis* but the mechanism of activation is poorly understood, in part because the binding interaction has not been properly established. The class I peroxidases ascorbate peroxidase (APX) and cytochrome *c* peroxidase (CcP) have active site structures very similar to KatG and are also capable of activating isoniazid. We report here the first crystal structures of complexes of isoniazid bound to APX and CcP. These are the first structures of isoniazid bound to any activating enzymes. The structures show that isoniazid binds close to the δ -heme edge in both APX and CcP, although the precise binding orientation varies slightly in the two cases. A second binding site for INH is found in APX at the γ -heme edge close to the established ascorbate binding site, indicating that the γ -heme edge can also support the binding of aromatic substrates. We also show that in an active site mutant of soybean APX (W41A) INH can bind directly to the heme iron to become an inhibitor and in a different mode when the distal histidine is replaced by alanine (H42A). These structures provide the first unambiguous evidence for the location of the isoniazid binding site in the class I peroxidases and provide rationalization of isoniazid resistance in naturally occurring KatG mutant strains of *M. tuberculosis*.

Isoniazid (isonicotinic acid hydrazide, INH,³) (Scheme 1) is a prodrug that has been extensively used as a frontline chemotherapeutic to treat tuberculosis for many years (1). More than

8 million people per year are diagnosed with tuberculosis in both developed and developing nations, resulting in more than 2 million deaths per year (2). However, despite the worldwide success of INH in treating tuberculosis since the 1950s, very little is understood about the mode of action or the mechanism of activation of this prodrug. In recent times the emergence of INH- and multidrug-resistant strains of tuberculosis and the scale of the tuberculosis epidemic has highlighted the need for this fundamental lack of knowledge to be addressed with a view to discovering new antimicrobial targets and treatment regimens.

In vitro and *in vivo* studies have established that a catalase peroxidase, KatG, which is endogenous to *M. tuberculosis* (the principal causative agent of tuberculosis), is essential for prodrug activation (3). KatGs are bifunctional heme enzymes that exhibit both catalase activity and broad spectrum peroxidatic activity comparable with monofunctional peroxidases (4, 5). The peroxidatic activity involves the formation of an oxidized ferryl intermediate (Equation 1, *Compound I*) that is subsequently reduced by substrate. This reduction usually occurs in two successive single-electron transfer steps as follows (Equations 2 and 3) (where *P* = peroxidase, *HS* = substrate, *S*[•] = 1-electron oxidized form of substrate).



KatG is a dimeric heme-containing enzyme of ~160-kDa molecular mass; its structure (Fig. 1A) (6) and function place it in the class I superfamily of peroxidases along with cytochrome *c* peroxidase (CcP) (Fig. 1B) and ascorbate peroxidase (APX) (Fig. 1C) (7). The determination of the crystal structure of *M. tuberculosis* KatG (6) provided a major breakthrough in understanding the molecular mechanism of INH activation and highlighted the remarkable structural similarity both in the overall structures and at the active sites of KatG and the monofunctional class I peroxidases such as CcP (8) and APX (9), both of

* This work was supported by Biotechnology and Biological Sciences Research Council Grants BBC/0011841 (to E. L. R. and P. C. E. M.), 91/B19083 (to E. L. R.), and BBS/S/A/2004/12421 (to E. L. R.). The costs of publication of this article were defrayed in part by the payment of page charges. This article must therefore be hereby marked "advertisement" in accordance with 18 U.S.C. Section 1734 solely to indicate this fact.

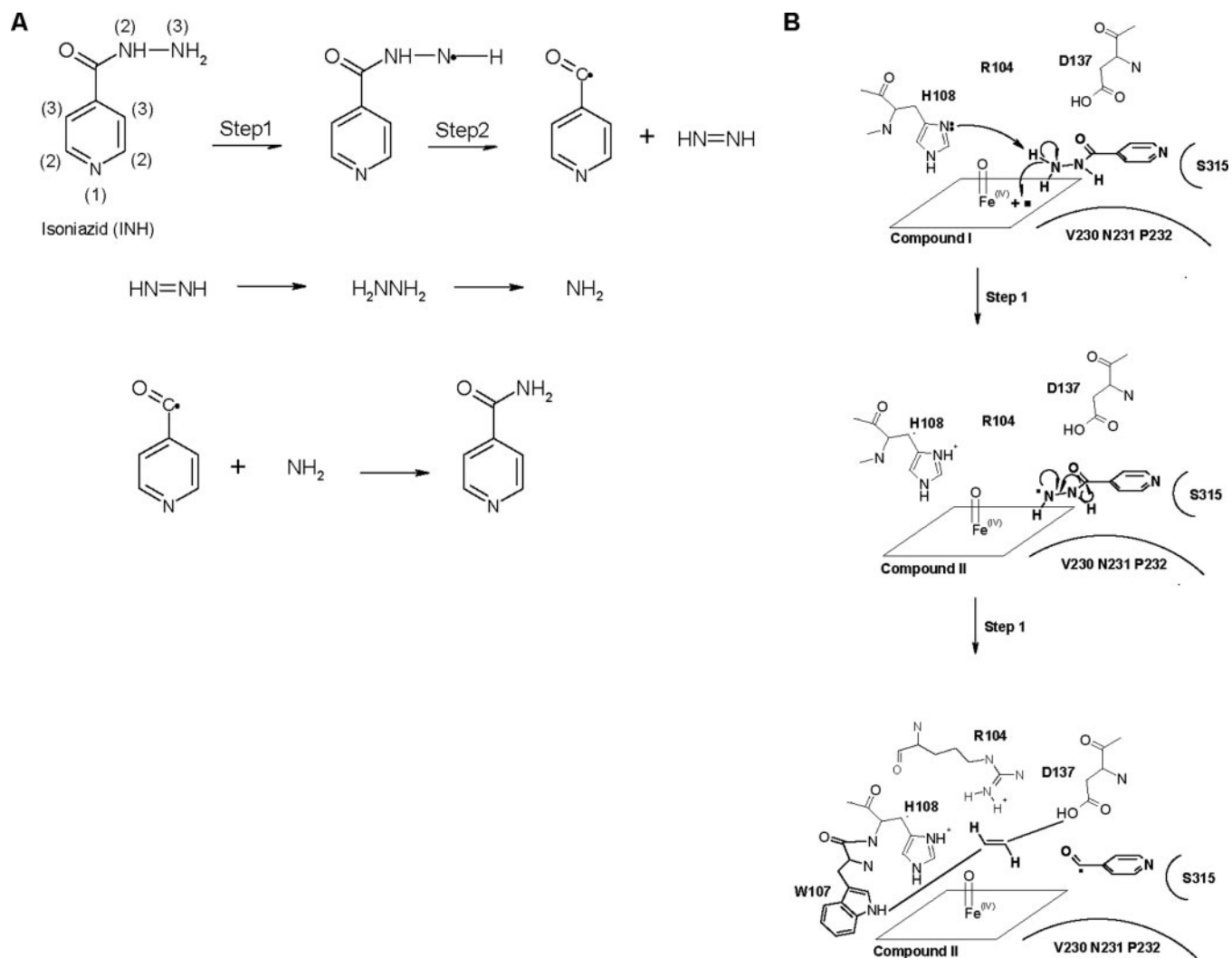
The atomic coordinates and structure factors (codes 2V23, 2V2E, 2VCF, 2VCN, and 2VCS) have been deposited in the Protein Data Bank, Research Collaboratory for Structural Bioinformatics, Rutgers University, New Brunswick, NJ (<http://www.rcsb.org/>).

¹ Present address: The Edward Jenner Inst. for Vaccine Research, Compton, Newbury, Berkshire RG20 7NN, UK.

² To whom correspondence should be addressed. Tel.: 44-116-229-7097; Fax: 44-116-229-7084; E-mail: peter.moody@le.ac.uk.

³ The abbreviations used are: INH, isonicotinic acid hydrazine; CcP, cytochrome *c* peroxidase; APX, ascorbate peroxidase; sAPX, soybean APX; SHA, salicylhydroxamic acid.

Isoniazid-activating Peroxidase Complexes



SCHEME 1. A, the proposed catalytic mechanism of INH oxidation by the class I peroxidases. The first stage (*steps 1 and 2*) forms the isonicotinoyl radical, which is then thought to react with the liberated hydrazine to form the primary product isonicotinamide (38). The INH numbering scheme is also shown. B, the active site residues of KatG that are proposed to be involved in the catalytic mechanism of INH oxidation (1). Possible stabilizing interactions are shown as *dotted lines*, and the heme is represented as a *rhombus*. The equivalent residues in CcP and sAPX are as follows: Arg-104 \equiv Arg-48, Arg-38; Trp-107 \equiv Trp-51, Trp-41; His-108 \equiv His-52, His-42; Asp-137 \equiv Ser-81, Ala-70. Asp-137 of KatG is thought to play a major role in stabilizing the catalytic intermediate of INH oxidation.

which can also activate INH (1) (Fig. 1). Mechanistic studies show INH is activated by both KatG and the class III peroxidase horseradish peroxidase in the typical two-step peroxidatic process, again indicating a universal mechanism of INH oxidation in peroxidases (1) (Scheme 1). In most peroxidases, aromatic substrates similar in structure to INH, such as salicylhydroxamic acid (SHA) (10) and benzhydroxamic acid (11), bind and react at the δ -heme edge. However, there is no direct structural information for INH binding from any of the INH-activating enzymes. The best information available on the INH binding site in peroxidases comes from an NMR model of INH bound to horseradish peroxidase. These NMR data were used as a basis for energetic grid calculations from which a set of models describing the INH binding site in KatG and other class I peroxidases were constructed. In all of these models the INH binding site was placed at the δ -heme edge in what is commonly referred to as the hydrophobic pocket (1).

To fully elucidate the mechanism of INH activation in KatG and other INH-activating peroxidases, the binding site of

INH has to be accurately described. Only then can the fine molecular details of catalysis be unraveled. Here we report the first crystal structures of INH bound to *Saccharomyces cerevisiae* CcP and soybean ascorbate peroxidase (sAPX), both of which are known activators of INH (1). We establish that the INH occupies the δ -meso edge of the heme, and we also show that in an active site mutant of sAPX (W41A) INH can bind directly to the heme iron to become an inhibitor. Furthermore, we show in a complex of INH and the H42A mutant of sAPX that the indole nitrogen of Trp-41 is important for ligand orientation. The data are discussed in the context of our current understanding of INH binding and activation and provide an explanation for the molecular mechanism of mutation-acquired resistance.

EXPERIMENTAL PROCEDURES

Enzyme Expression and Purification—The Y39A/N184R mutant of recombinant CcP from Baker's yeast (optimized for crystallization) was prepared and isolated with modifications to

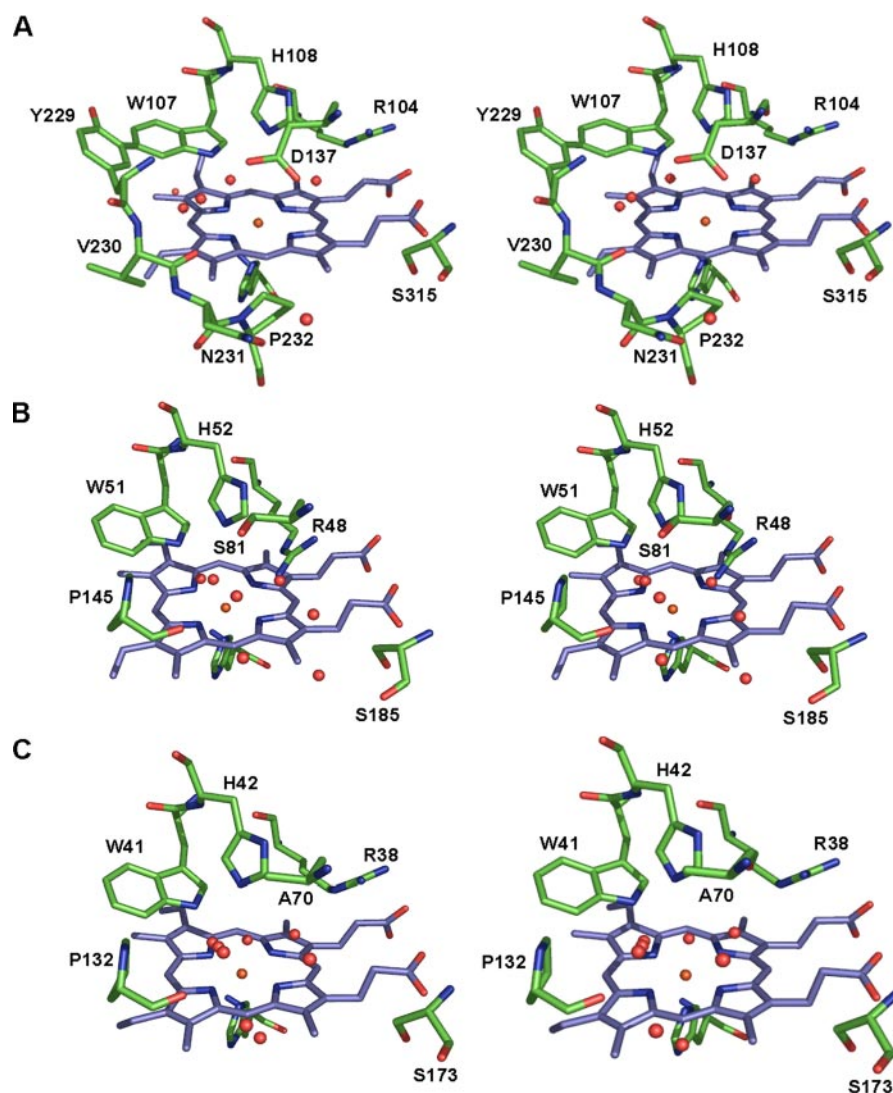


FIGURE 1. Stereo diagrams of the key active site residues, δ -heme edge hydrophobic binding pocket, and bound waters of the unliganded class I peroxidases discussed in this study. KatG (6) (A), CcP (9) (B), and sAPX (9) (C). The protein residues are shown in green, the heme group in blue, and waters are represented as red spheres.

TABLE 1
Data collection and refinement statistics

Values in parentheses are for the outer shell.

Data collection	CcP ^a	CcP-INH ^a	sAPX-INH	sAPX(W41A)-INH	sAPX(H42A)-INH ^a
Space group	P2 ₁ -2 ₁ -2 ₁	P2 ₁ -2 ₁ -2 ₁	P4 ₂ 2 ₁ 2	P4 ₂ 2 ₁ 2	P4 ₂ 2 ₁ 2
Unit cell (Å)					
a	51.15	51.15	82.24	82.13	81.74
b	75.38	75.13	82.24	82.13	81.74
c	107.23	106.86	74.97	75.16	74.94
Resolution (Å)	30.2-1.68 (1.77-1.68)	30.28-1.68 (1.77-1.68)	27.11-1.80 (1.90-1.80)	37.58-1.20 (1.26-1.20)	27.62-1.68 (1.77-1.68)
Total observations	101429 (1628)	129214 (1652)	170464 (24801)	732420 (82637)	103919 (1437)
Unique reflections	37067 (1317)	38990 (1367)	24461 (3497)	78730 (11128)	24816 (1102)
<i>I</i> / σ <i>I</i>	23.2 (3.3)	27.4 (5.8)	17.4 (4.7)	17.2 (2.5)	31.2 (2.5)
<i>R</i> _{merge}	0.036 (0.238)	0.031 (0.133)	0.091 (0.378)	0.063 (0.687)	0.032 (0.209)
Completeness (%)	77.7 (19.7)	81.9 (20.3)	100 (100)	97.9 (96.0)	84.0 (26.8)
Refinement statistics					
<i>R</i> _{work}	0.159	0.156	0.154	0.192	0.165
<i>R</i> _{free}	0.192	0.180	0.188	0.209	0.209
Root mean square deviations from ideal					
Bonds (Å)	0.012	0.010	0.012	0.007	0.010
Angles (°)	1.208	1.157	1.234	1.151	1.174
Protein Data Bank code	2V23	2V2E	2VCF	2VCN	2VCS

^a These figures are for data measured into the corners of the square detector and used for refinement. In the case of CcP, CcP-INH, and sAPX (H42A) INH, the completeness to 2.0 Å is, respectively, 92.9, 99.3, and 99.6%.

published procedures (12). Recombinant cytosolic sAPX and the W41A and H42A mutants were prepared and isolated according to published procedures (13, 14). All protein preparations were checked for homogeneity by SDS-PAGE.

Protein Crystallography—Crystals of CcP were prepared by microdialysis with 100 μ l of a 10–30 mg/ml solution of CcP in 500 mM potassium phosphate, pH 6.0, against 10 ml of 50 mM potassium phosphate, pH 6.0, containing 30% 2-methyl-2,4-pentanediol by volume. Crystals were grown at 4 °C. Once formed, the crystals of CcP were soaked in mother liquor saturated with INH for 5 min prior to rapid cooling to 100 K.

Crystals of sAPX, sAPX (W41A), and sAPX (H42A) were prepared as described previously (9). Once formed, crystals were soaked in mother liquor containing INH (100 mM) overnight prior to freezing in liquid nitrogen for storage and transport.

Data Collection and Refinement—Diffraction data were collected for the CcP-INH complex in-house using a Rigaku RU2HB x-ray generator with copper anode and Xenocs multilayer optics and an R-Axis IV detector. Diffraction data were collected for sAPX-INH and sAPX (W41A) INH complexes

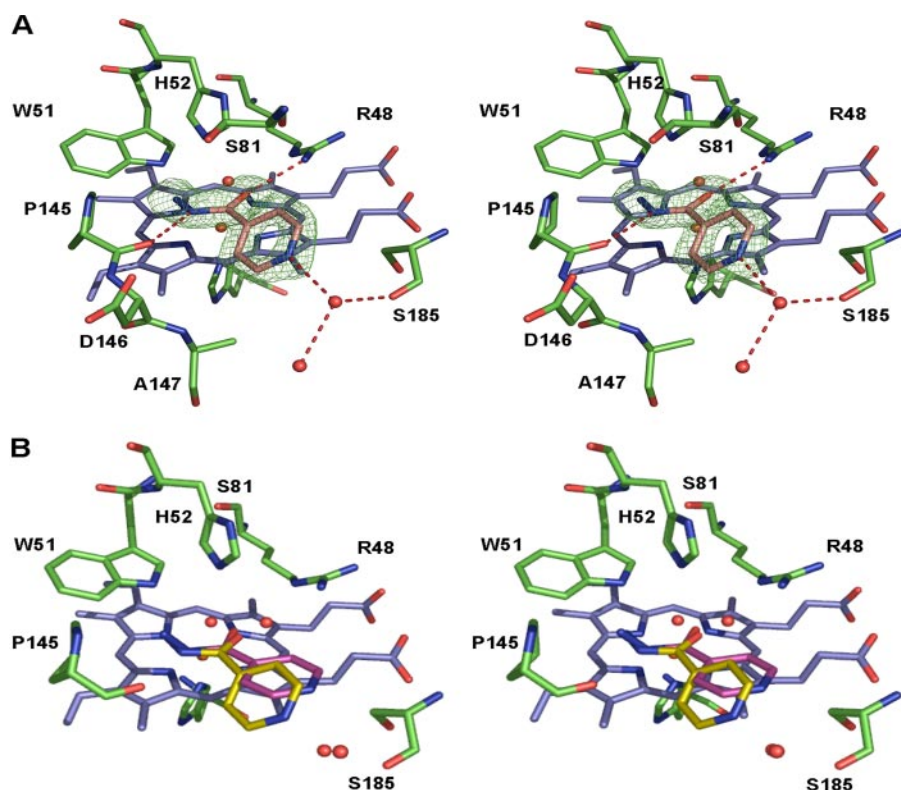


FIGURE 2. Stereo diagrams showing INH bound in place of waters in the δ -heme edge hydrophobic binding pocket of CcP. A, observed $F_o - F_c$ difference density is shown in green (contoured at 3σ) with the refined INH molecule in brown. B, the observed position of INH (yellow) compared with the predicted mode (purple) from Pierattelli *et al.* (1). The protein is shown in green, the heme group in blue, INH in pink, and waters are represented as red spheres.

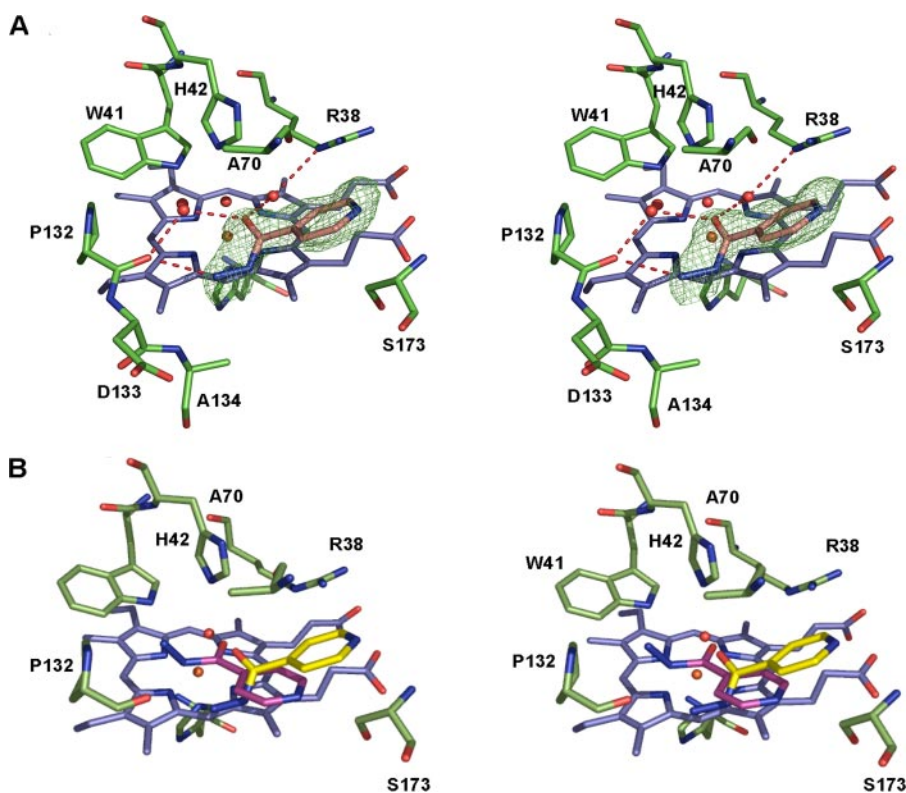


FIGURE 3. Stereo diagrams showing INH bound in place of waters in the δ -heme edge hydrophobic binding pocket of sAPX. A, observed $F_o - F_c$ difference density in green (contoured at 3σ) with the refined INH molecule in brown. B, the observed position of INH (yellow) compared with the predicted mode (purple) from Pierattelli *et al.* (1). The protein is shown in green, the heme group in blue, INH in pink, and waters are represented as red spheres.

on station ID14-3 at the European Synchrotron Radiation Facility (ESRF) (Grenoble, France) using an ADSC Q4R detector. Data from sAPX·(H42A)·INH were also collected at ESRF using ID14-1 and an ADSC Q4R detector. All data were collected at 100 K. Data were indexed, integrated, and scaled using MOSFLM (15) and SCALA (16). 5% of the data were flagged for the calculation of R_{free} and excluded from subsequent refinement. Data collection statistics are shown in Table 1. The CcP·INH structure was refined from the 1.70 Å wild-type CcP structure (17) (Protein Data Bank entry 2CYP). The sAPX·INH and sAPX (H42A)·INH structures were refined from models derived from the 1.45 Å sAPX·ascorbate complex (9) (Protein Data Bank entry 1OAF), and the sAPX (W41A)·INH structure was derived from the 1.35 Å sAPX·W41A structure (14) (Protein Data Bank entry 2GGN). All refinement used REFMAC5 (18) from the CCP4 suite (19). Calculation of difference Fourier maps showed clear and unambiguous electron density for bound INH molecules in all the structures. INH was incorporated into the last cycles of refinement. COOT (20) was used throughout for manual adjustment, ligand fitting, and interpretation of the water structure. The refinement statistics are shown in Table 1.

Steady-state Kinetic Experiments—Steady-state oxidations of guaiacol (2-methoxy phenol) in 50 mM sodium phosphate, pH 7.0, 25 °C, were carried out according to published protocols (21) both in the absence of INH and in the presence of INH (50 mM). Steady-state data were fitted either to the Michaelis-Menten or Hill equations as described previously (21).

RESULTS AND DISCUSSION

Identification of the Hydrophobic Binding Pockets in CcP and sAPX—Numerous studies have shown that aromatic substrate oxidation in the class I peroxidases occurs at the δ -heme edge (6, 11, 23, 24). This site

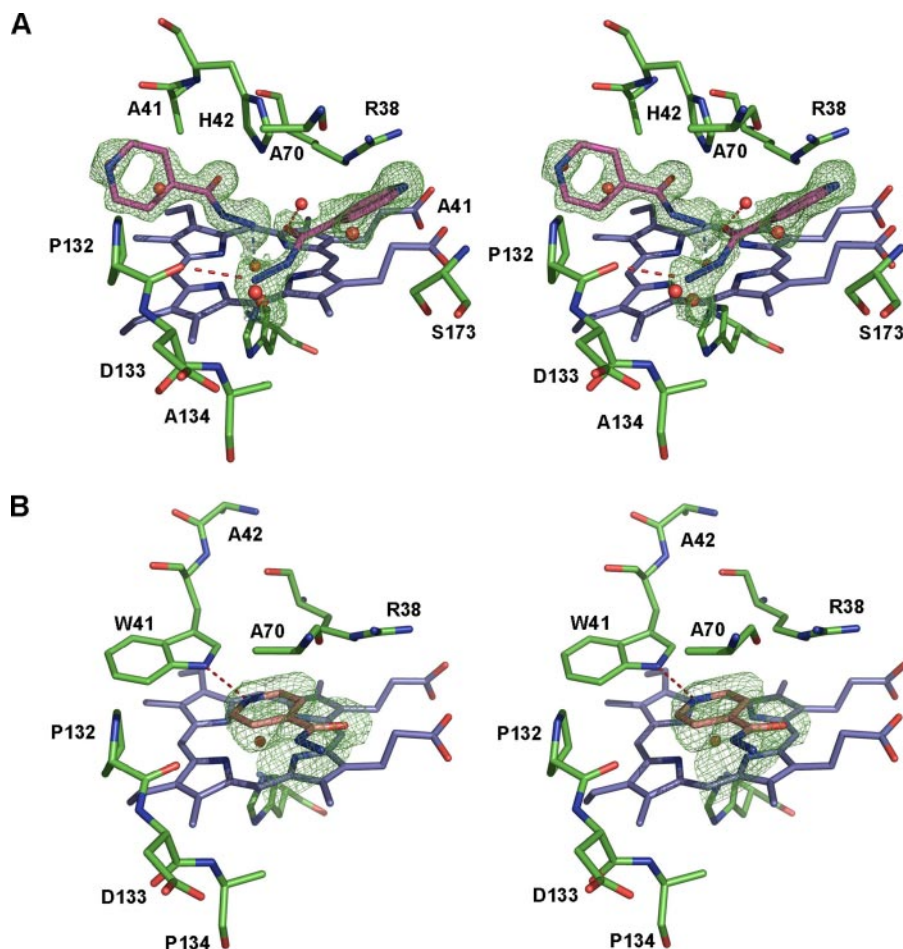


FIGURE 4. Stereo diagrams showing INH bound in the active site mutants of sAPX W41A and H42A. *A*, in sAPX(W41A), two molecules of INH (brown) are bound in the distal cavity, one in the same position as sAPX and a second coordinated directly to the heme iron. The figure shows observed $F_o - F_c$ difference density (in green, contoured at 3σ). *B*, in sAPX(H42A) the orientation of INH (brown) is rotated relative to the wild type and is held in position by a hydrogen bond to Trp-41. Observed $F_o - F_c$ difference density is shown in green. In both cases the occupancy of the INH is partial and shared with water molecules that are represented as red spheres.

is compared in KatG, CcP, and sAPX in Fig. 1. In the unliganded CcP structure the hydrophobic pocket itself is defined, as predicted from the crystal structure (17), by residues Pro-145, Ser-81, Ser-185, Arg-48, Trp-51, and His-52, with the “bottom” of the pocket being defined by pyrrole ring IV of the heme while one “side” is left open to solvent (Fig. 1*B*). Examination of electron density within this pocket in CcP reveals water molecules hydrogen-bonded within the pocket and leading out into bulk solvent. This open side forms a channel to allow the substrate to access the binding pocket.

The unliganded sAPX structure (Fig. 1*C*) shows an almost identical active site architecture with the hydrophobic pocket defined by Trp-41, His-42, Pro-132, Ser-173, and Ala-70, and again the bottom of the pocket is defined by pyrrole ring IV of the heme. Like CcP (17) and KatG (6), ordered water molecules occupy this pocket in sAPX with a substrate access channel leading to bulk solvent. Thus, the pockets in all three of these class 1 peroxidases are similar and available to bind hydrophobic aromatic substrates.

The Structures of INH Bound to CcP and sAPX—INH binds in place of four of the water molecules within the hydropho-

bic pocket of CcP (Fig. 2*A*). The structure allows hydrogen bonds between N2 of the substrate and the main chain oxygen of Pro-145, the carbonyl oxygen on the substrate and the side chain of Arg-48, and the pyridinyl nitrogen on the substrate and a water molecule leading out to bulk solvent. The guanidinium group of Arg-48 swings out to accommodate the substrate ($C\zeta$ moves by 2 Å) and displaces a further water molecule. The overall position of the INH in the crystal structure reported here is similar to the NMR-derived model (Fig. 2*B*) (1) except for the interactions of N2 and N3. Notably, the crystal structure is inconsistent with a predicted (1) hydrogen bond between the globally conserved distal tryptophan (Trp-51 in the case of CcP) and N3 of INH.

The structure of sAPX in complex with INH also shows INH bound in the hydrophobic pocket at the δ -meso heme edge (Fig. 3*A*). However, in this case the INH is rotated through $\sim 90^\circ$ compared with the orientation in CcP and the predicted sAPX·INH model (Fig. 3*B*) (1). The pyridine ring of INH is positioned directly over Ser-173, and the complex is locked into position via three hydrogen bonds, two of which are to the same residues

that are used to bind INH in CcP. The main chain carbonyl of Pro-132 hydrogen bonds to N3 of the INH, the carbonyl oxygen of INH hydrogen bonds via a water molecule to the Ne group of Arg-48, and the N2 of INH is hydrogen-bonded to a water molecule.

Previous mechanistic studies have proposed a KatG-catalyzed activation mechanism that involves splitting of the C–N bond of the hydrazide moiety of INH, yielding a diazene that is stabilized by Asp-137 (Scheme 1) (1, 6). In *M. tuberculosis* KatG the acid group of Asp-137 is predicted to be located directly above the carbonyl of INH and is ideally orientated to provide a stabilizing acid-base interaction with the reacting INH. However, in CcP and sAPX, Asp-137 is replaced with Ser-81 and Ala-70, respectively. Ser-81 could still offer some rudimentary stabilization for the activated INH, whereas this is unlikely with Ala-70. This hypothesis is supported by the relative reaction rates of INH oxidation, $KatG \gg Ccp > sAPX$ (1).

The Structures of INH Bound to sAPX Mutants W41A and H42A and the Role of Point Mutations in Drug Resistance—A major problem in treating tuberculosis is resistance to the clinically effective drugs rifampicin and INH. Various point muta-

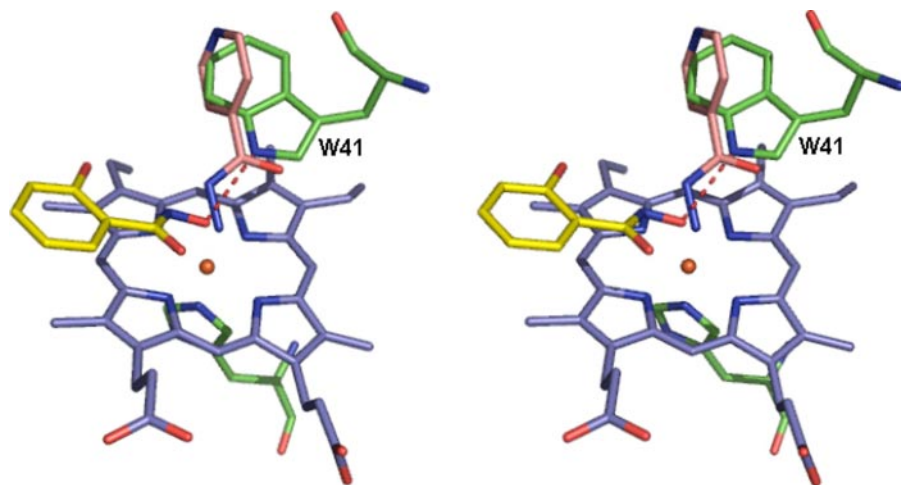


FIGURE 5. Stereo diagram showing the superposition of INH binding as an inhibitor of sAPX-W41A (pink) with the previously determined SHA binding orientation (yellow) in sAPX (10). The hydrogen bond between the coordinating oxygen of SHA and Trp-41 is shown as a broken red bond. An analogous hydrogen bond cannot form between the coordinating NH_2 of INH and Trp-41, so that coordination is only possible when Trp-41 is absent in sAPX (W41A).

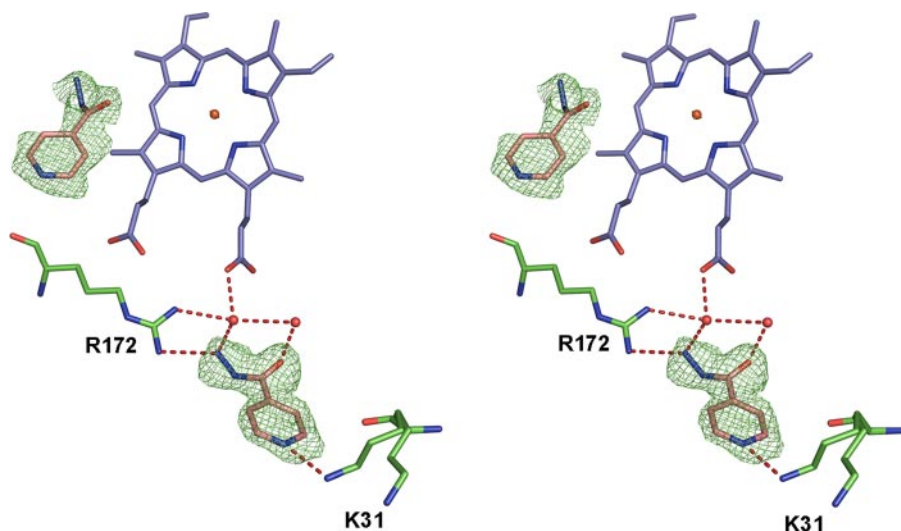


FIGURE 6. Stereo diagram showing INH bound in the ascorbate binding pocket of sAPX. Hydrogen bonding interactions are observed between INH and Arg-172 and Lys-31 and via a water to the propionate group of the heme. There are INH molecules bound in identical positions in the sAPX (W41A) and sAPX (H42A) structures. The first INH molecule bound in the distal cavity is also shown to aid orientation. The protein is shown in green, the heme group in blue, and INH in pink. Waters are represented as red spheres. The observed $F_o - F_c$ difference density (contoured at 3σ) for the INH molecules is shown in green. Figs. 2–6 were prepared with PyMOL (22).

tions of KatG have been identified in INH-resistant strains (25), with one of the mutation hotspots being Ser-315 (mutated to asparagine, isoleucine, arginine, and glycine, but most commonly threonine) (26–28). Ser-315 is conserved in both CcP and sAPX (Fig. 1) as Ser-185 and Ser-173, respectively. In the CcP·INH structure the $C\alpha$ of Ser-185 is ~ 4.0 Å from the aromatic ring of INH, and in sAPX the $C\beta$ of Ser173 is ~ 3.8 Å away and located directly below it. All of these mutations would introduce considerably more steric bulk than serine, thereby placing the side chain of the mutated residue at position 315 closer than allowed Van der Waal's contact distances, blocking the binding of the INH molecule. These observations are consistent with predictions that these mutations produce a steric interference to INH binding (6, 29).

Active site residues His-108 and Ala-110 are also frequently mutated in KatG sequenced from isolates demonstrating resistance to INH (30–32). Mutation of active site residues of peroxidases has been shown (14) to introduce conformational mobility into the distal cavity, possibly promoting alternative inhibitive INH binding orientations. To probe this, we have determined the structures of INH bound to two active site mutations of sAPX (W41A and H42A). Removal of the distal tryptophan in the W41A mutant of sAPX opens up the distal cavity and imparts a degree of conformational mobility (14). Electron density from crystals of INH-soaked sAPX (W41A) shows a molecule of INH occupying the hydrophobic pocket in an identical position to that found in the wild-type sAPX·INH complex. A second INH molecule is also seen coordinated directly to the heme iron through the NH_2 of the acyl hydrazide, with the aromatic ring occupying the pocket created by removal of the indole of Trp-41 (Fig. 4A). This mode of binding has been seen previously (10) in APX for aromatic acids such as SHA, which is an inhibitor of APX peroxidase activity. However, coordination of INH to the iron is only possible when an additional pocket is created in the W41A mutant, whereas coordination of SHA is possible with Trp-41 *in situ* (10). This is because SHA forms a hydrogen bond between its iron coordinating O^- and the NH of Trp-41 (Fig. 5). However, INH has an NH_2 group coordinated to the iron that is unable to hydrogen bond to the NH of Trp-41; furthermore, its bulk would also result in a steric clash. The removal of Trp-41 allows the INH to move around through 90° to coordinate to the iron without this steric conflict (Fig. 5). Kinetic studies show that INH becomes an inhibitor of sAPX (W41A) peroxidase activity, determined by competition with guaiacol (k_{cat} for guaiacol oxidation is $98.3 \pm 1.2 \text{ s}^{-1}$ in the absence of INH compared with $5.0 \pm 0.04 \text{ s}^{-1}$ in the presence of 50 mM INH). These observations are consistent with the structure of sAPX (W41A)·INH that shows INH bound directly to the heme iron; thus, in solution the reaction of the enzyme with H_2O_2 is blocked by preventing the formation of the compound I intermediate (by a mechanism similar to that proposed for SHA) (10).

The structure of INH bound to the H42A mutant of sAPX reveals a third binding orientation of INH within the distal cavity (Fig. 4B). In this structure the INH again occupies the δ -heme edge but is rotated 90° anticlockwise compared with the orientation in sAPX. The removal of His-42 creates enough space for the aromatic ring of INH to sit directly above the iron and hydrogen bond through N1 to the NH of Trp-41. This provides further evidence that Trp-41 influences coordination to the heme iron. Although the cavity in sAPX·H42A can contain the INH molecule, the steric clash with Trp-41 (see Fig. 5) prevents coordination. Kinetic studies show no INH turnover by sAPX (H42A) (data not shown); however, it has been previously shown that peroxidase activity in this mutant (21) is severely reduced. A reduction in INH activation is consistent with the observation of INH resistance in *M. tuberculosis* strains with mutations at the distal His-108 residue of KatG (30, 31).

Occupation of the Ascorbate Binding Site of sAPX by INH—The electron density maps of INH-soaked sAPX (Fig. 6) and mutants (data not shown) also show density consistent with a second INH molecule bound within the ascorbate binding pocket at the γ -heme edge, which has previously been identified as the primary site of catalysis within the enzyme (9) (Fig. 6). The INH molecule binds in place of six well ordered water molecules that occupy the pocket in the absence of ascorbate. The NH₂ group of INH forms two hydrogen bonds, one to the side chain of Arg-172 and one via a water molecule to one of the heme propionate groups. The flexible Lys-31 also partially swings in from solvent to form a hydrogen bond to N1 of INH. Movement of Lys-31 on binding of ascorbate has also been observed (9). The role of the heme propionates has traditionally been believed to be in stabilizing the heme prosthetic group within the protein structure. However, there are now several examples where the heme propionates are involved in substrate or cofactor binding, notably in manganese peroxidase (33), ascorbate peroxidase (9), and in nitric-oxide synthase (34–36); this has led to the suggestion (37) that there might be a broader role for the propionates than merely keeping the heme in place. The data above add to this by indicating, for the first time, that the γ -heme edge might also be capable of binding aromatic substrates.

In summary, we have provided unambiguous structural evidence for the location of INH binding in the class I peroxidases CcP and sAPX. These data expand on previous predictions and provide a molecular understanding of prodrug binding and activation. Furthermore, by comparing mutations engineered into our peroxidase models with naturally occurring INH-resistant variants of *M. tuberculosis*, we have identified three separate means of drug resistance: steric hindrance of the δ -heme edge INH binding site, direct binding to the heme iron (and consequent inhibition of compound I formation), and the loss of peroxidatic activity due to the mutation of essential catalytic residues. Finally, we have expanded the framework of understanding for aromatic substrate binding and activation in the heme peroxidases. We have shown that single point mutations can dramatically alter substrate binding and oxidation, indicating that the sites may be more promiscuous than previously thought. These observations provide a fundamental platform

upon which our understanding of the enzyme-catalyzed activation of this prodrug can now be developed for more effective tuberculosis therapies in the future.

Acknowledgments—We thank staff at the European Synchrotron Radiation Facility, Grenoble for providing synchrotron time and Sandip Badyal for providing crystals of sAPX-(W41A).

REFERENCES

- Pierattelli, R., Banci, L., Eady, N. A. J., Bodiguel, J., Jones, J. N., Moody, P. C. E., Raven, E. L., Jamart-Gregoire, B., and Brown, K. A. (2004) *J. Biol. Chem.* **279**, 39000–39009
- World Health Organization (2002) Vallanjohn, M., ed *Report on Infectious Diseases*, Geneva
- Zhang, Y., Heym, B., Allen, B., Young, D., and Cole, S. (1992) *Nature* **358**, 591–593
- Nagy, J. M., Cass, A. E. G., and Brown, K. A. (1997) *J. Biol. Chem.* **272**, 31265–31271
- Johnsson, K., Froland, W. A., and Schultz, P. G. (1997) *J. Biol. Chem.* **272**, 2834–2840
- Bertrand, T., Eady, N. A. J., Jones, J. N., Nagy, J. M., Jamart-Gregoire, B., Raven, E. L., and Brown, K. A. (2004) *J. Biol. Chem.* **279**, 38991–38999
- Welinder, K. G. (1992) *Curr. Opin. Chem. Biol.* **2**, 388–393
- Poulos, T. L., Freer, S. T., Alden, R. A., Edwards, S. L., Skogland, U., Takio, K., Eriksson, B., Xuong, N., Yonetani, T., and Kraut, J. (1980) *J. Biol. Chem.* **255**, 575–580
- Sharp, K. H., Mewies, M., Moody, P. C. E., and Raven, E. L. (2003) *Nat. Struct. Biol.* **10**, 303–307
- Sharp, K. H., Moody, P. C. E., Brown, K. A., and Raven, E. L. (2004) *Biochemistry* **43**, 8644–8651
- Henriksen, A., Schuller, D. J., Meno, K., Welinder, K. G., Smith, A. T., and Gajhede, M. (1998) *Biochemistry* **37**, 8054–8060
- Fishel, L. A., Villafranca, J. E., Mauro, J. M., and Kraut, J. (1987) *Biochemistry* **26**, 351–360
- Lad, L., Mewies, M., and Raven, E. L. (2002) *Biochemistry* **41**, 13774–13781
- Badyal, S. K., Joyce, M. G., Sharp, K. H., Seward, H. E., Mewies, M., Basran, J., Macdonald, I. K., Moody, P. C. E., and Raven, E. L. (2006) *J. Biol. Chem.* **281**, 24512–24520
- Leslie, A. G. W. (1992) *Joint CCP4 + ESF-EAMCB Newsletter on Protein Crystallography*, No. 26 Daresbury Laboratory, Warrington, UK
- Evans, P. R. (2005) *Acta Crystallogr. Sect. D Biol. Crystallogr.* **62**, 72–82
- Finzel, B. C., Poulos, T. L., and Kraut, J. (1984) *J. Biol. Chem.* **259**, 13027–13036
- Murshudov, G. N., Vagin, A. A., and Dodson, E. J. (1997) *Acta Crystallogr. Sect. D Biol. Crystallogr.* **53**, 240–255
- Bailey, S. (1994) *Acta Crystallogr. Sect. D Biol. Crystallogr.* **50**, 760–763
- Emsley, P., and Cowtan, K. (2004) *Acta Crystallogr. Sect. D Biol. Crystallogr.* **60**, 2126–2132
- Lad, L., Mewies, M., Basran, J., Scrutton, N. S., and Raven, E. L. (2002) *Eur. J. Biochem.* **369**, 3182–3192
- DeLano, W. L. (2002) *The PyMOL Molecular Graphics System*, DeLano Scientific, San Carlos, CA
- Itakura, H., Oda, Y., and Fukuyama, K. (1997) *FEBS Lett.* **412**, 107–110
- Tsukamoto, K., Itakura, H., Sato, K., Fukuyama, K., Miura, S., Takahashi, S., Ikezawa, H., and Hosoya, T. (1999) *Biochemistry* **38**, 12558–12568
- Heym, B., Alzari, P. M., Honore, N., and Cole, S. T. (1995) *Mol. Microbiol.* **15**, 235–245
- Cockerill, F. R., Uhl, J. R., Temesgen, Z., Zhang, Y., Stockman, L., Roberts, G. D., Williams, D. L., and Kline, B. C. (1995) *J. Infect. Dis.* **171**, 240–245
- Haas, W. H., Schilke, K., Brand, J., Amthor, B., Weyer, K., Fourie, P. B., Bretzel, G., StichtGroh, V., and Bremer, H. J. (1997) *Antimicrob. Agents Chemother.* **41**, 1601–1603
- Marttila, H. J., Soini, H., Eerola, E., Vyshnevskaya, E., Vyshnevskiy, B. I., Otten, T. F., Vasilyef, A. V., and Viljanen, M. K. (1998) *Antimicrob. Agents Chemother.* **42**, 2443–2445
- Kapetanaki, S., Chouchane, S., Giroto, S., Yu, S. W., Magliozzo, R. S., and

Isoniazid-activating Peroxidase Complexes

- Schelvis, J. P. M. (2003) *Biochemistry* **42**, 3835–3845
30. Rouse, D. A., Li, Z. M., Bai, G. H., and Morris, S. L. (1995) *Antimicrob. Agents Chemother.* **39**, 2472–2477
31. Rouse, D. A., and Morris, S. L. (1995) *Infect. Immun.* **63**, 1427–1433
32. Musser, J. M., Kapur, V., Williams, D. L., Kreiswirth, B. N., van Soolingen, D., and van Embden, J. D. A. (1996) *J. Infect. Dis.* **173**, 196–202
33. Sundaramoorthy, M., Kishi, K., Gold, M. H., and Poulos, T. L. (1994) *J. Biol. Chem.* **269**, 32759–32767
34. Raman, C. S., Li, H. Y., Martasek, P., Kral, V., Masters, B. S. S., and Poulos, T. L. (1998) *Cell* **95**, 939–950
35. Crane, B. R., Arvai, A. S., Ghosh, D. K., Wu, C. Q., Getzoff, E. D., Stuehr, D. J., and Tainer, J. A. (1998) *Science* **279**, 2121–2126
36. Fischmann, T. O., Hruza, A., Niu, X. D., Fossetta, J. D., Lunn, C. A., Dolphin, E., Prongay, A. J., Reichert, P., Lundell, D. J., Narula, S. K., and Weber, P. C. (1999) *Nat. Struct. Biol.* **6**, 233–242
37. Poulos, T. L. (2007) *Nat. Prod. Rep.* **24**, 504–510
38. Bodiguel, J., Nagy, J. M., Brown, K. A., and Jamart-Gregoire, B. (2001) *J. Am. Chem. Soc.* **123**, 3832–3833

The Tuberculosis Prodrug Isoniazid Bound to Activating Peroxidases
Clive Metcalfe, Isabel K. Macdonald, Emma J. Murphy, Katherine A. Brown, Emma
Lloyd Raven and Peter C. E. Moody

J. Biol. Chem. 2008, 283:6193-6200.

doi: 10.1074/jbc.M707412200 originally published online December 5, 2007

Access the most updated version of this article at doi: [10.1074/jbc.M707412200](https://doi.org/10.1074/jbc.M707412200)

Alerts:

- [When this article is cited](#)
- [When a correction for this article is posted](#)

[Click here](#) to choose from all of JBC's e-mail alerts

This article cites 35 references, 15 of which can be accessed free at
<http://www.jbc.org/content/283/10/6193.full.html#ref-list-1>